Salen-manganese complexes for controlling ROS damage: Neuroprotective effects, antioxidant activity and kinetic studies[§]

Lara Rouco,[a] Andrea Liberato,[b] M. Jesús Fernández-Trujillo,[b] Angeles Máñez,[b] Manuel G. Basallote,[b,*] Rebeca Alvariño,[c] Amparo Alfonso,[c] Luis M. Botana,[c,*] and Marcelino Maneiro[a,*]

[a] Departamento de Química Inorgánica, Facultade de Ciencias, Campus Terra, Universidade de Santiago de Compostela, Lugo, Spain;

[b] Departamento de Ciencia de los Materiales e Ingeniería Metalúrgica y Química Inorgánica, Facultad de Ciencias, Universidad de Cádiz, Puerto Real, Cádiz, Spain;

[c] Departamento. de Farmacología, Facultade de Veterinaria, Campus Terra, Universidade de Santiago de Compostela, Lugo, Spain.

Corresponding author: Phone: 34 982824106; Fax: 34 982285872

E-mail: marcelino.maneiro@usc.es

[§] In memory of the late Professor Juan Manuel Salas, an inspiring force for Spanish bioinorganic chemists

Abstract

A new manganese(III) complex [$MnL^1(DCA)(H_2O)](H_2O)$, **1**, has been prepared using the chelating ligand *N*,*N'*-bis(2-hydroxy-3-methoxybenzylidene)-1,2-diaminopropane (H_2L^1), and characterized by different analytical and spectroscopic techniques. The tetragonally elongated octahedral geometry for the manganese coordination sphere was revealed by X-ray diffraction studies for **1**. The antioxidant behavior of this complex and other manganese(III)-salen type complexes was tested through SOD and catalase probes, and through the study of their neuroprotective effects in SH-SY5Y neuroblastoma cells. In this human neuronal model, these model complexes were found to improve cell survival in an oxidative stress model. During studies aimed to getting a better understanding of the kinetics of the processes involved in this antioxidant behavior, an important effect on the solvent in the kinetics of reaction of the complexes with H_2O_2 was revealed that suggests a change in the mechanism of reaction of the complexes. The kinetic data in methanol and buffered aqueous solutions correlate well with the results of the test of catalase activity, thus showing that the rate determining step in the catalytic cycle corresponds to the initial reaction of the complexes with H_2O_2.

Keywords

Manganese; Oxidative Stress; Neuroprotection; Schiff bases

1. INTRODUCTION

Reactive oxygen species (ROS) like superoxide radical anion ($O_2^{\bullet-}$), hydrogen peroxide (H_2O_2) or hydroxyl radical ($OH^{\bullet}$), are generated as by-products of mitochondrial electron

transport of aerobic respiration [1]. ROS levels are regulated by antioxidant enzymes as superoxide dismutases (SOD), catalases (CAT), and glutathione peroxidases (GPx) [2]. An imbalance in this oxidant-antioxidant status could determine the extent of cell damage, which is particularly risky for brain cells that are susceptible to oxidative damage due to their high rate of energy consumption, and other factors as the relative low levels of brain antioxidant defences or the high concentrations of polyunsaturated fatty acids in this organ. Excessive ROS levels have been associated with neurodegenerative disorders like Alzheimer`s Disease (AD), Parkinson's Disease (PD), amyotrophic lateral sclerosis (ALS) or Huntington`s Disease [3-4]. All these neurodegenerative diseases may shorten life span, but, most notably, they affect the life quality of aging populations causing cognitive deficits, memory loss, and behavioural alterations [5]. For instance, AD has already become a healthcare challenge facing our society today: According to the new report, the loss of cognitive abilities provoked by AD currently accounts for 50 million cases worldwide, but this number will be more than triple to 150 million by 2050 [6]. In this context, efforts have been directed toward the search of antioxidant enzyme mimics [7-9]. This research determination has often focused on manganese complexes with Schiff bases as Mn ions do not induce Fenton chemistry [10-16]. It is well established that these complexes protect cells from oxidative damage in animal models and lead to benefits in AD and PD, stroke, motor neuron disease, multiple sclerosis, and excitotoxic neural injury [17-19]. However, the mechanism of action of these biomimetic models remain exiguously understood. They have been reported as antioxidant agents which can behave as SOD, catalases or peroxidases mimics, but more studies are needed for a more comprehensive understanding of underlying molecular mechanisms and associated pathophysiological pathways.

We have previously reported a number of these biomimetic models and tried to delineate the functional roles of the bridging ligands and structural motifs that play a key role in their antioxidant activity [20-23]. Thus, we have found how the combination of hydrogen bonding networks and π-aryl interactions would lead to active self-assembled μ-aquo dimeric systems [20-24], and also we have established an increase of the catalytic activity for this type of biomimetic models in function of the tetragonal elongation (ratio between the manganese-axial donor atom distances and the manganese-equatorial donor atom distances) of the octahedral manganese complexes [21]. This elongation occurs when the degeneracy is broken by the stabilization (lowering in energy) of the d orbitals with a *z* component, while the orbitals without a *z* component are destabilized (higher in energy). The tetragonal elongation enhances the lability of an axial position where the substrate molecule can be subsequently accommodated in this site, following an inner-sphere electron-transfer mechanism. As a result, complexes with square-pyramidal or tetragonally elongated octahedral geometries turn into efficient biomimetic catalysts for ROS control [22-25].

In the work described here, we further explored this scheme. For this purpose, we selected the dianionic H_2L^1-H_2L^3 Schiff base ligands (Scheme 1; *N*,*N'*-bis(2-hydroxy-3-methoxybenzylidene)-1,2-diaminopropane, H_2L^1; *N*,*N'*-bis(2-hydroxy-3-methoxybenzylidene)-1,2-diaminoethane, H_2L^2; and *N*,*N'*-bis(2-hydroxy-3-methoxybenzylidene)-1,2-diamino-2-methylpropane, H_2L^3), which contains four potential donor atoms: two imine nitrogen atoms and two phenolic oxygen atoms. The insertion of the outer methoxy groups would favour the aggregation of neighbouring complexes through hydrogen bonding in order to get dimeric systems. The inductive electron donating effect of the methoxy group also may facilitate to achieve high-valent manganese centres during

catalysis. Moreover, we selected a bulky ancillary ligand like dicyanamide ions in order to favour a higher tetragonal elongation for the manganese complex, which is expected to increase the lability thus favouring reaction with oxidants. We examined the cytoprotective effect of the resulting complexes **1**-**3** against H_2O_2-induced oxidative stress in human neuroblastoma cells. Human neuroblastoma SH-SY5Y cells have been widely used as a cell model system for studying oxidative stress [26-27], even though this paper report for the first time the neuroprotective results of Mn(III)-Schiff base complexes for this human neuronal model. Finally, we performed kinetic studies of the reaction of complexes **1**-**3** versus H_2O_2 and tertbutyl hydroperoxide (TBHP), aimed at unravelling some clues for their mode of action in their antioxidant activity.

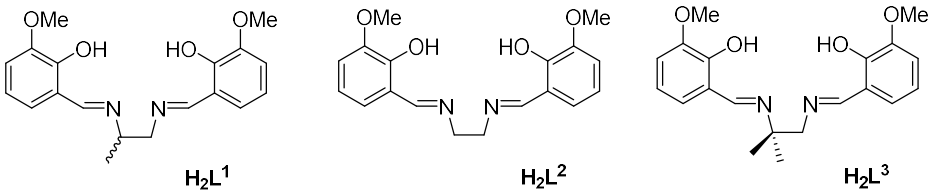

Scheme 1. Sctructures for H_2L^1-H_2L^3.

2. EXPERIMENTAL SECTION

2.1. Materials for synthesis and chemical reactions. All solvents, 3-methoxy-2-hydroxybenzaldehyde, ethylenediamine, 1,2-diaminepropane, 1,2-diamine-2-methylpropane, manganese(II) acetate, sodium dicyanamide, hydrogen peroxide and TBHP are commercially available and were used without further purification.

Schiff base ligands H_2L^1-H_2L^3 for complexes **1**-**3** were prepared according to the literature [28] by condensation of 3-methoxy-2-hydroxybenzaldehyde and the corresponding diamine in methanol, and their synthesis and characterization have been already reported [21]. Complexes **1**-**3** were also synthesized according to the literature; complexes **2**, $Mn_2L^2_2(H_2O)_2(DCA)_2$, and **3**, $MnL^3(H_2O)_2(DCA)$, have been previously obtained [29-30], where DCA is the dicyanamide ion. Experimental procedure and characterization data for **1** are collected below:

Comentado [M1]: aqui

$MnL^1(H_2O)_2(DCA)$ (**1**) To a methanolic solution of 0.675 mmol (0.25 g) of H_2L^1, 0.675 mmol (0.17 g) of $Mn(CH_3COO)_2$ was added and the stirred solution changed its initial yellow colour to brown. After 30 minutes of stirring with gentle heating, 0.675 mmol (0.06 g) of $NaN(CN)_2$ in 10 mL of methanol was added. The solution was then concentrated by slow evaporation. The complex was obtained as brown crystals, which were isolated by filtration, washed with diethyl ether and dried in air. Yield 58%. Anal. Calcd. for $C_{21}H_{24}MnN_5O_6$ (497.4): C, 50.7; H, 4.8; N, 14.1. Found: C, 50.5; H, 4.6; N, 14.5 %. MS ES (m/z) 395 $[MnL]^+$, 462 $[MnL(DCA)]^+$; IR (KBr, cm^{-1}): v(O-H) 3422, v(C=N) 1624, v(C-O) 1260, ν_{sym}(C≡N) 2149, ν_{asym}(C≡N) 2251; ^{1}H NMR (DMSO-d_6, ppm): δ -17.3 (H4), -24.7 (H5). μ = 4.9 BM. $E_{1/2}$ = -72 mV. ΔE_p = 110 mV. Λ_M = 45 μS.

2.2. Physical and analytical measurements for compound characterization. Elemental analyses were performed on a Carlo Erba Model 1108 CHNS-O elemental analyser. The IR spectra were recorded as KBr pellets on a Bio-Rad FTS 135 spectrophotometer. ^{1}H NMR spectra were recorded on a Bruker AC-300 spectrophotometer using DMSO-d_6 as solvent and $SiMe_4$ as an internal reference. The electrospray mass spectra of the compounds were obtained on a Hewlett-Packard model LC-MSD 1100 instrument. Room-temperature

magnetic susceptibilities were mesasured using a digital measurement system MSB-MKI, calibrated using mercury tetrakis(isothiocyanato)cobaltate(II) as a susceptibility standard. Electronic spectra were recorded on a Cary 230 spectrometer. Conductivities of 10^{-3} M solutions in DMF were measured on a Crison microCM 2200 conductivemeter. Electrochemical measurements were performed using an EG&G Princeton Applied Research model 273 potentiostat using three electrode configuration. The working electrode was a Metrohm model 6.1204.000 graphite disc while a Pt wire and a saturated calomel electrode served as counter and reference electrodes, respectively. Measurements were made with *ca.* 10^{-3} M solutions of complexes in DMF using 0.1 M ~~mol dm^{-3}~~ tetraethylammonium perchlorate as a supporting electrolyte.

Comentado [M2]: aqui

Comentado [M3]: aqui

Con formato: Tachado

2.3. Studies on catalase-like function. A 10 mL flask containing the solution of the complexes in methanol (3 mL, 1 mM) was sealed with septum and connected to a gas-measuring burette (precision of 0.1 mL) through double-ended needle. The solution was stirred at constant temperature on a water bath. The catalysis was initiated by introducing H_2O_2 solution (1 mL, 2.5 M) using syringe, and the evolved dioxygen was volumetrically measured.

2.4 Cell Culture. All the experiments were performed as previously described [27]. Human neuroblastoma SH-SY5Y cell line was purchased from the American Type Culture Collection (ATCC), number CRL2266. The cells were maintained in Dulbecco's modified Eagle's medium: Nutrient Mix F-12 (DMEM/F-12) supplemented with 10% foetal bovine serum

(FBS), glutamax, 100 U/mL penicillin and 100 µg/mL streptomycin at 37 °C in a humidified atmosphere of 5% CO_2 and 95% air. Cells were dissociated weekly using 0.05% trypsin/EDTA. All reagents were provided by Thermo Fisher Scientific (Waltham, MA, USA).

2.5. Cell Viability Assay. One day prior to experiments, cells were seeded in 96-well plates at a density of 5 × 10^4 cells per well. SH-SY5Y cells were treated with biomimetic models **1**-**3** at different concentrations (0.001, 0.01, 0.1, 1 and 10 µM) for 24 h. The effect of compounds on cell viability was evaluated by MTT (3-(4, 5-dimethyl thiazol-2-yl)-2,5-diphenyl tetrazolium bromide) assay [31-32].SH-SY5Y cells were rinsed with saline solution and 200 µL of MTT (500 µg/mL) dissolved in saline buffer were added to each well. Following 1 h of incubation at 37 °C, SH-SY5Y cells were disaggregated with 5% sodium dodecyl sulphate. Absorbance of formazan crystals was measured at 595 nm with a spectrophotometer plate reader. Saponin from quillaja bark was used as a death control and its absorbance was subtracted from the other data.

2.6. Superoxide dismutase activity assay. The SODs levels were analysed with SOD assay kit (Sigma-Aldrich). SH-SY5Y were seeded in 24 well plates at a density of 1 x 10^5 cells per well. Cells were co-treated with biomimetic models **1**-**3** and EUK-134 at different concentrations (0.001, 0.01, 0.1, 1 and 10 µM) for 24 h. Cells were washed with ice-cold PBS and 50 µL of lysis buffer (0.1 M Tris- HCl, pH 7.4 containing 0.5% Triton X-100, 5 mM β-mercaptoethanol and 0.1 mg/mL PMSF) were added to each well. The SOD assay was performed following manufacture's protocol. SODs activity was normalized by protein concentration, which was quantified by Bradford method. Half maximal effective

concentration (EC50) values were calculated using a non-linear regression model with Graph Pad Prism 6 software.

2.7. Neuroprotection and Mitochondrial Membrane Potential Assays. The ability of compounds to protect cells from TBHP damage was also evaluated with MTT probe. Cells were co-treated with complexes **1**-**3** at non-toxic concentrations (0.001, 0.01, 0.1, 1 and 10 μM) and 75 μM TBHP for 6 h, and the assay was carried out as described above. All experiments were performed at least three times. The mitochondrial membrane potential (ΔΨm) was assessed using the tetramethylrhodamine methyl ester (TMRM) probe. SH-SY5Y cells were seeded in 96-well plates at a density of 5×10^4 cells per well and allowed to attach for 24 h. After this time, cells were treated with 75 μM TBHP and biomimetic models **1**-**3** at different concentrations (0.001, 0.01, 0.1 and 1) for 6 h. Cells were washed twice with saline solution and 1 μM TMRM was added to each well for 30 min at 37 °C. After incubation, cells were solubilised with DMSO and H_2O at 50% and the fluorescence was monitored with a spectrophotometer plate reader (535 nm excitation and 590 nm emission). All experiments were performed at least three times. The endogenous antioxidant vitamin E (vitE) at 25 μM was used to validate the *in vitro* model in all the assays. Data are presented as mean ± SEM. Statistical differences were evaluated by Student´s *t*-tests with Graph Pad Prism 6 software. Statistical significance was considered at $p < 0.05$.

2.8. Kinetic experiments. The kinetic experiments using a conventional spectrophotometer were carried out with a Cary 50 Bio UV/Vis spectrophotometer provided with a multicell accessory. The stopped-flow experiments were carried out with an Applied Photophysics SX18-MV instrument provided with a PDA diode array detector. Experiments in acetonitrile

and methanol solvents were carried out at 25.0±0.1 ºC by mixing a solution of the Mn complexes with a solution containing an excess of H_2O_2; the final concentrations in the resulting mixture were 5×10^{-5} M for the complex and (0.6 - 5.0) $\times10^{-2}$ M for the oxidant. Experiments in aqueous solution were carried out at 37.0±0.1 ºC by mixing 0.1 ml of a solution of the Mn complexes in DMSO (1×10^{-6} M) with 2.4 mL of an aqueous solution buffered at pH= 7.25 containing an excess of H_2O_2 or TBHP; the final concentration of the complex was 1×10^{-6} M and the oxidant was in the range (0.08 – 9.0) $\times10^{-3}$ M. In all cases, the spectral changes were measured over a wide wavelength range and analyzed with the program Specfit [33] using the kinetic models indicated in the next sections.

2.9. Crystallographic studies. Single crystals of complex **1**, suitable for X-ray diffraction studies, were obtained by slow evaporation of the methanolic solution at room temperature. Table 1 collects detailed crystal data collection and refinement for **1**. Measurements were made on a Bruker X8 APEXII CCD diffractometer employing graphite-monochromated *Mo-Kα* radiation at 100 K. The structures were solved by direct methods [34] and finally refined by full-matrix least- squares base on F^2. An empirical absorption correction was applied using SADABS [35]. All non-hydrogen atoms were assigned anisotropic displacement parameters in the refinement. The hydrogen atoms were included in the model at geometrically calculated positions.

Refinement of F^2 against ALL reflections. The weighted R-factor wR is based on F2, conventional R-factors R are based on F, with F set to zero for negative F^2. The threshold expression of $F^2 > 2\sigma(F^2)$ is used only for calculating R-factors(gt) etc. and is not relevant to the choice of reflections for refinement. R-factors based on F^2 are statistically about twice

as large as those based on F, and R- factors based on ALL data will be even larger.

Table 1. Crystal data and structure refinement for complex **1**.

Comentado [M4]: aqui insertado espacios

	Complex **1**
Chemical formula	$C_{21}H_{30}MnN_5O_5$
Formula weight	487.44
Crystal system	Monoclinic
Space group	$P2_1/c$
Temperature (K)	100(2)
a (Å)	13.3896(18)
b (Å)	12.8009(17)
c (Å)	13.8265(18)
α (°)	90
β (°)	112.767(6)
γ (°)	90
Volume (Å^3)	2185.2(5)
Z	4
Radiation type	Mo *K*α
μ (mm^{-1})	0.648
Crystal size (mm)	0.40 x 0.17 x 0.03
Theta range for data collection	1.649 to 25.414º
F (000)	1024
No. of measured reflections	30054
No. independent reflections	4005
Goodness-of-fit on F^2	1.035
R [$F^2 > 2\sigma(F^2)$]	0.0776
wR(F^2)	0.1731
No. of parameters	373
$\Delta)_{max}$, $\Delta)_{min}$ (e Å^{-3})	0.690, -0.815

3. RESULTS AND DISCUSSION

3.1. Synthesis and characterization of complex 1

Complex **1** was obtained in high yield as detailed in the experimental section. Metal complexation was evidenced by the change in the color of the solution, from yellow to brown. Elemental analysis establishes a formula $MnL^1(DCA)(H_2O)_2$, other analytical and spectroscopic techniques support such formula and give insights into the structure of the complex. Thus, conductivity measurements in 10^{-3} M dimethylformamide solutions are in agreement with non-electrolyte behavior [36]; magnetic moment value at room temperature are very close to the spin-value of 4.9 B.M., as expected for a high-spin magnetically diluted d^4 manganese(III) ion; ESI-mass spectrum shows the formation of the manganese complex.

pParamagnetic ^{1}H NMR spectrum with two upfield proton resonances due to the isotropically shifting of the ligand protons for high-spin manganese(III) complexes in an octahedral field. The data interpretation of this technique was based on previous findings for manganese(III) complexes with related Schiff base ligands [20-22]. The signals must arise from the H4 and H5 protons of the aromatic phenoxy rings. Signals in ortho positions to donor atoms are not observable for these kinds of complexes by paramagnetic ^{1}H NMR spectroscopy[37]

IR spectrum for **1** exhibits a strong band at 1624 cm^{-1} characteristic of the v(C=N) stretching mode, which is shifted 9 cm^{-1} lower respect to the free Schiff base ligand, indicating the coordination to the manganese through the nitrogen atoms of the imine group. The band attributed to the v(C-O) mode at 1260 cm^{-1} is shifted 10 cm^{-1} to higher frequencies respect

to the free ligand. Moreover, two new bands at 2149 and 2251 cm^{-1} are assigned, respectively, to the symmetric and asymmetric dicyanamide modes [38].

The electronic spectrum indicates that the Mn(III) complex behaves as high-spin octahedral d^4 system that probably suffers a significant Jahn-Teller distortion. The band at around 330-350 nm can be assigned to an intraligand π-π transition [15]. A broad band at 440 nm is attributable to the phenolate → Mn(III) charge-transfer [39].

The electrochemical properties of complexes **1**-**3** were investigated by cyclic voltammetry (data is collected in Table 3, and figures of the voltammograms are available in the Supporting Information section, Figure S4). The three complexes exhibit one Mn^{III}/Mn^{II} quasi-reversible wave, with peak to peak separation in the range 110 to 196 mV. The low $E_{1/2}$ values in the range -72 to -141 mV are in accordance with the electron-donor character for the methoxy substituents on the phenolato rings. The potentials are lower by 200-400 mV than the potentials of the corresponding complexes without methoxy substituents or including electron-withdrawing substituents [21]. Thus, the electron-donor character of the methoxy groups on the phenyl rings of the Schiff base facilitates to achieve higher oxidation states for the manganese ion during catalysis [7,40].

Single crystals of complex **1** suitable for X-ray diffraction studies were obtained by slow evaporation of the methanolic solution at room temperature. The crystal structure is shown in Figure 1 and main bond distances and angles are shown in Table 2.

The monomeric unit is composed by a distorted octahedron, where the $(L^1)^{2-}$ ligand is tightly bound to the metal ion through the inner N_2O_2 compartment by the N_{imine} and O_{phenol} atoms (Mn-N_{imine} bond lengths of 1.972(6)-1.974(19) Å and Mn-O_{phenol} of 1.868(5)-1.877(4) Å, which are typical of such complexes [21-22]), occupying the equatorial positions. The axial

positions are occupied by a monodentate dicyanamide ligand and a water molecule. The axial distances of 2.240(4) Å (for Mn-O(1W)) and 2.272(19)-2.29(3) Å (for Mn-N(31)) are considerably longer than the equatorial Mn-O bond lengths quoted earlier, resulting in a expected tetragonal elongation for the solid state structure already suggested by the electronic spectrum in solution. The authors' intent was to achieve such distorted geometry in order to get labile positions that subsequently facilitate vacancy positions for catalytic purposes. Previous reported complexes incorporing DCA show Mn-Oax/Mn-Oeq ratios of about 1.22 [24,30], which are significantly higher than values of about 1.15 obtained for other similar Mn-Schiff base compounds [21]. In the case of **1**, this ratio of about 1.20 implies a significant tetragonal elongation but the value is not as high as expected for the effect derived from the introduction of the DCA ligand [21,30]. In this sense, a key point to achieve high tetragonal elongations is the short two-carbon chain between imine groups in the Schiff base ligand (like in H_2L^1-H_2L^3) as this short chain constricts the chelate ring once nitrogen atoms coordinate to the metal.

Table 2. Selected bond lengths (Å) and angles (º) for complex **1**.

Mn(1)-O(27)	1.868(5)	Mn(1)-O(17)	1.877(4)
Mn(1)-N(2)	1.972(6)	Mn(1)-N(6)	1.974(19)
Mn(1)-N(31A)	2.272(19)	Mn(1)-O(1W)	2.240(4)
Mn(1)-N(31B)	2.29(3)		
O(27)-Mn(1)-O(17)	92.92(18)	O(27)-Mn(1)-N(6)	92.0(2)
O(27)-Mn(1)-N(2)	174.6(2)	O(17)-Mn(1)-N(6)	174.8(2)
O(17)-Mn(1)-N(2)	92.1(2)	N(2)-Mn(1)-N(6)	83.0(2)
O(27)-Mn(1)-O(1W)	92.12(18)	O(17)-Mn(1)-O(1W)	91.80(17)
O(1W)-Mn(1)-M(31A)	171.5(9)	O(27)-Mn(1)-N(31A)	96.1(8)

Both Schiff base ligand and dicyanamide ligand show disordered positions. The aliphatic chain of $(L^1)^{2-}$ present two different configurations. The main configuration, labelled as C3A-C5A, has a parameter occupancy of 78(2) %, and the complementary configuration present a value of 22(2) %. For the case of the dicyanamide, also with two different configurations, their respective values are 59.6(8) % for N31A-N35A, and 40.4(8) % for N31B-N35B.

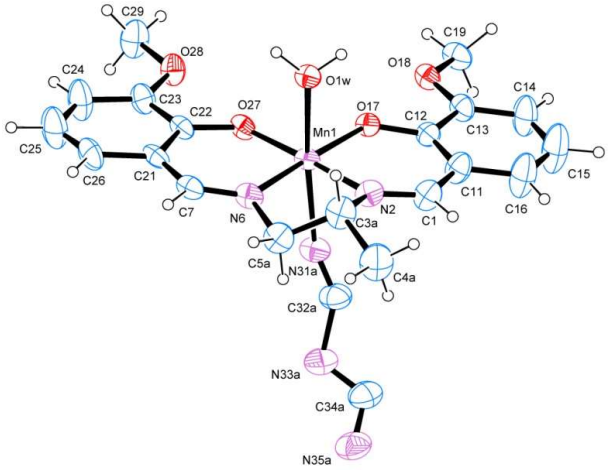

Figure 1. ORTEP view of the environment around the manganese ion in complex **1**

The superstructure of **1** involves associations via a combination of π-aryl offset interactions [41] and hydrogen bonding. Hydrogen bonding represents a class of weaker, non-covalent interactions that not only induce supramolecular arrays through self-organization of molecules, but also plays a crucial role in fundamental biological processes, such as the expression and transfer of genetic information, and is essential for molecular recognition

between receptors and substrates [42]. Hydrogen bonds between capping water molecules and both phenoxy and methoxy oxygen atoms of the neighboring Schiff base ligand are formed. As result of all these non-covalent interactions complex **1** present a μ-aqua dimeric structure (Figure 2), with Mn···Mn distances of about 4.9 Å are short for monomeric compounds.

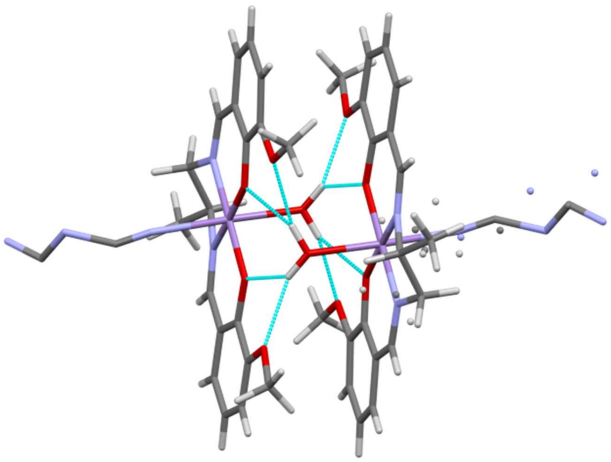

Figure 2. Stick diagram for the dimeric unit for complex **1** (manganese ion in magenta, oxygen in red, nitrogen in blue, and carbon in grey)

3.2. Catalase and superoxide dismutase activities

We have checked the CAT of **1**-**3** in methanolic solutions. ~~For the case of the CAT studies, we have measured~~ the stoichiometry of the disproportionation of H_2O_2 catalysed by **1**-**3** by volumetric determination of the evolved O_2. The experimental setup was evaluated by the

Comentado [M5]:

Comentado [M6]: activity?

Comentado [M7]: ...solutions by measuring the stoichiometry...

Con formato: Tachado

measurements for the catalytic decomposition of H_2O_2 (2.5 x 10^{-3} mol) with MnO_2: *ca.* 30 mL of dioxygen evolution was measured by a burette, which agrees with the calculated value based on the assumption that catalytic decomposition of H_2O_2 to H_2O and O_2 takes place. Table 3 collects the results of the CAT activities. The time course of oxygen production is similar for each of the complexes. The reaction proceeds quickly during the first 5-10 min and over time the total amount of oxygen evolved approaches an asymptotic limit. Complexes **1**-**3** achieve percentages of H_2O_2 dismutation from 23 to 27%, althought this type of CAT assay only gives a semiquantitative approach about the activity of the complexes. A detailed kinetic study for the reaction of **1**-**3** with hydrogen peroxide is discussed in section 3.4 of this paper.

Table 3. Redox potentials, SOD and catalase activities for **1**-**3**. (a) half wave potential; (b) peak-to-peak separation; (c) catalase activity expressed as percentage of H_2O_2 decomposed after 60 min, (d) SOD activity expressed as half maximal effective concentration (EC50) values; R^2 is the coefficient of determination which gives the goodness-of-fit for the regression model.

Complex	**$E_{1/2}$ (mV)[a]**	**ΔEp[b]**	**Catalase activity[c]**	**SOD activity**	
				EC50 (nM)[d]	**R^2**
1	-72	110	27 ± 3	9.876	0.99
2	-141	111	23 ± 2	10.540	0.93
3	-75	196	24 ± 2	155.100	0.98

The effect of complexes and EUK-134 on SODs activity was assessed in human neuroblastoma cells. The concentration of $O_2^{\bullet-}$ was determined with WST-1 [2-(4-

Comentado [M8]: aqui

Con formato: Tachado

Iodophenyl)-3-(4-nitrophenyl)-5-(2,4-disulfophenyl)-2H-tetrazolium, monosodium salt], which reacts with the ROS to produce a water soluble formazan dye, that was determined by a colorimetric method. Therefore, SODs activity is inversely related to WST signal. Cells were treated with different concentrations of compounds for 24 h, and their effect on SODs enzymatic activity was evaluated. Then, EC50 values were determinated (Figure S5 collects SOD activity curves). EUK-134 presented an EC50 of 28.45 nm (R^2 = 0.95), an activity lower than complexes **1** and **2** (Table 3). Complex **1** showed the best results (9.876 nm), a SOD activity value three times better than the commercial EUK-134.

3.3. Protective effect of complexes 1-3 on TBHP-treated SH-SY5Y cells

At first, the cytotoxicity of complexes was determined in SH-SY5Y cells, which were treated with different concentrations of complexes **1**-**3** (Figure 3) (0.001- 10 μM) for 24 h. None of the compounds presented cytotoxic effects at these concentrations.

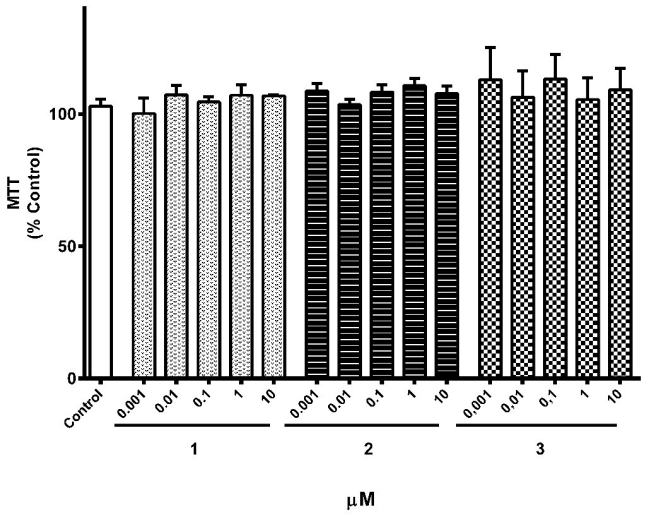

Figure 3. Cell viability of cells treated with **1**-**3**. Human neuroblastoma cells were treated with compounds for 24 h and their cytotoxic effects were determined with MTT assay. Values are mean ± SEM of three independent replicates, expressed as percentage of untreated control cells.

For oxidative stress studies, TBHP was used as oxidant instead of hydrogen peroxide (a oxidant that has been widely used to produce oxidative injury in SH-SY5Y cells [43]) to induce cell damage due to its higher stability in physiological media [44]. Cells were co-treated with **1**-**3** at four concentrations (0.001-1 μM) and 75 μM TBHP for 6 h, and the effect of the compounds on cell viability was evaluated by MTT (Figure 4). Cell survival decreased about 50 % when cells were treated with 75 μM TBHP alone ($p < 0.01$). In order to validate the oxidative stress model, vitE was used as positive control and, as Figure 4 shows, it increased cell survival until untreated cells levels (100 ± 6 %). Treatment with complexes **1**-**3** significantly augmented the cell survival reduction produced by TBHP, with levels between 80 ± 5 % and 95 ± 8%, compared to TBPH control cells.

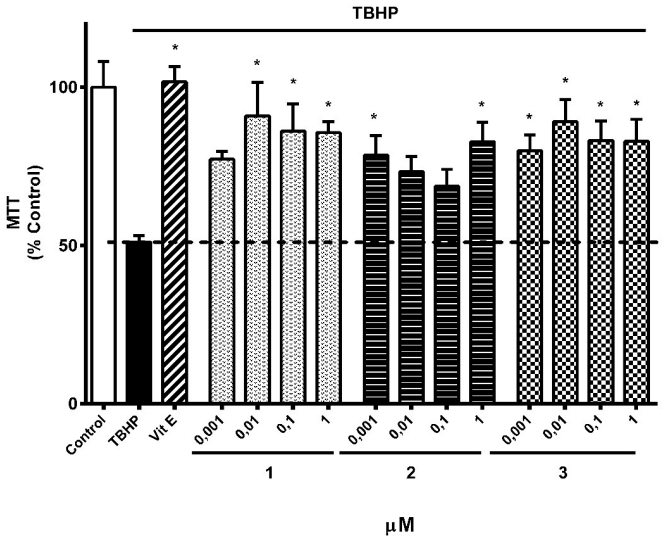

Figure 4. Neuroprotective effect of **1-3** in an oxidative stress model. SH-SY5Y cells were co-treated with 75 µM TBHP and compounds (0.001-1 µM) for 6 h. Then, their effect on cell viability was assessed by MTT test. Data are mean ± SEM of three experiments performed by triplicate. Values are expressed as percentage of control cells and compared to cells treated with TBHP alone by Student's *t* test. *$p < 0.05$

The effects of the biomimetic models **1**-**3** on mitochondrial functioning were determined with TMRM assay. TMRM is a fluorescent dye that enters in mitochondria and accumulates in inverse proportion to $\Delta\Psi_m$, so depolarized organelles will produce a lower signal. Neuroblastoma cells were co-treated with the compounds (0.001- 1 µM) and 75 µM TBHP for 6 h. TBHP addition produced a decrease in $\Delta\Psi_m$ of 30 % compared to control cells ($p < 0.01$) (Figure 5). Complexes **1** and **2** had no effect on the restoration of $\Delta\Psi_m$, and complex

3 had effect at the lowest concentration tested, with an increase of 106 ± 3 % at 0.001 μM. This percentage is greater than the levels reached by cells co-treated with 25 μM vitE.

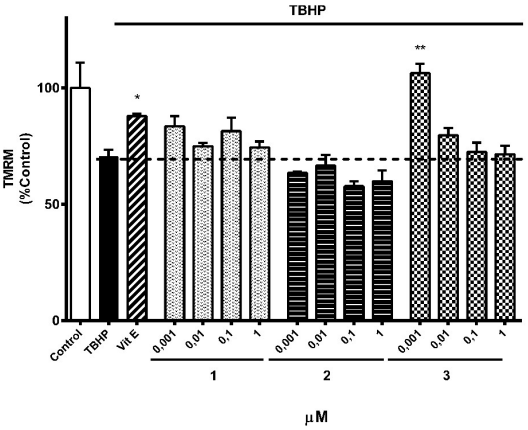

Figure 5. Effect of **1**-**3** on ΔΨm levels in human neuroblastoma cells. TBHP (75 μM) and compounds (0.001-1 μM) were added to the cells for 6 h. The fluorescence dye TMRM was used to evaluate their effect on ΔΨm. Mean ± SEM of three independent experiments. Data are expressed as percentage of control cells and compared to cells treated with TBHP alone. *p< 0.05, **p< 0.01

Our results indicate that **3** is the most promising compound, being able to protect cells from oxidative damage and ameliorate the mitochondrial function in a human neuronal model, so it may be a good candidate for further studies in neurodegenerative disorders such as AD.

3.4. Kinetic Studies.

Since the three complexes **1**-**3** can meaningfully improve the mitochondrial function, kinetic studies of their reaction with H_2O_2 and TBHP have been performed in different conditions.

In previous studies we found that the reaction of H_2O_2 and different Mn(III)-Schiff base biomimetic models, including EUK-134 (reported as a SOD, peroxidase and CAT mimic, tested against different oxidative pathologies and commercialized as a potent antioxidant [10,11,13,12,19]), in acetonitrile solutions are strongly dependent on the illumination conditions [23], suggesting the occurrence of a photochemical process. Similar studies have been now performed for complex **1**, and again the time scale of the spectral changes observed in the ABTS test for **1** in acetonitrile is significantly different when the kinetics is monitored with a stopped-flow instrument and a conventional spectrophotometer. In addition, no spectral changes are observed when the stopped-flow experiments are carried out using a 455 nm cut-on long pass filter. The effect of the illumination conditions is also observed for the reaction of the complex with H_2O_2, which occurs in the time scale of thousands of minutes with the conventional spectrophotometer and hundreds of seconds with the stopped-flow instrument (Figure S6). Photochemical processes prevent obtaining reliable kinetic data for the reaction in acetonitrile even from the spectral changes recorded with the conventional spectrophotometer, where the amount of incident light is minimized. In those cases, the spectral changes show frequently an induction period followed of slower and irreproducible spectral changes.

At that point, and given the SOD, peroxidase and CAT activity of EUK-134 and complexes **1**-**3** in other solvents, we decided to check if the behaviour observed in acetonitrile changes with the solvent. For this reason, studies parallel to those described above were carried out in methanol and in water, in the latter case using buffered solutions similar to those used in the biological studies. These experiments did not show the striking effect of the illumination conditions observed in acetonitrile solutions, the results obtained with the stopped-flow and the conventional spectrophotometer being comparable. However, as the reaction is slow, it

is not completed in the stopped-flow time scale and the kinetics was measured from the spectral changes observed with the conventional spectrophotometer.

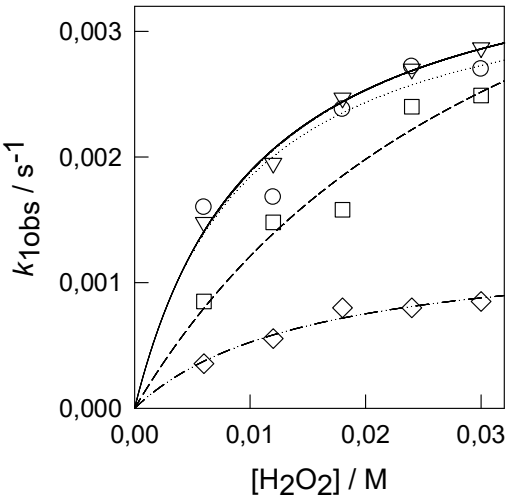

Figure 6. Plot of the [H_2O_2] dependence of the first observed rate constant in the reaction of the Mn complexes with H_2O_2 in methanol at 25 ºC: **1** (circles), **2** (triangles), **3** (squares), **EUK-134** (diamonds).

Table 4. Summary of kinetic data for the reaction of the Mn complexes with H_2O_2 in methanol solution at 25 ºC. For the meaning of *a* and *b* see equation 4.

	k_{1obs}		
Complex	***a*/s^{-1}**	***b*/M^{-1}**	**k_{2obs}/s^{-1}**
1	(3.6±0.6)×10^{-3}	(1.0±0.5)×10^{2}	(5.1±0.9)×10^{-5}
2	(3.8±0.2)×10^{-3}	(0.9±0.1)×10^{2}	[a]

3	$(5\pm2)\times10^{-3}$	$(0.3\pm0.2)\times10^{3}$	$(2.5\pm0.3)\times10^{-5}$
EUK-134	$(1.3\pm0.2)\times10^{-3}$	$(0.7\pm0.2)\times10^{3}$	$(1.2\pm0.3)\times10^{-5}$

[a] Curvature is observed in the plots of k_{2obs} vs. $[H_2O_2]$ and fitting to equation 4 leads to a= $(4.2\pm0.5)\times10^{-4}$ s^{-1} and b= $(0.8\pm0.2)\times10^{2}$ M^{-1}.

The spectral changes observed for the reaction of the Mn complexes with H_2O_2 in methanol show the disappearance of the bands typical of the starting complex, apparently without the appearance of any new band. An adequate fit of these spectral changes requires of a kinetic model with two consecutive steps, with rate constants k_{1obs} and k_{2obs} (A→B→C, see Figures S7-S8 for an example of spectral changes and calculated spectra for A, B and C). The dependence of k_{1obs} with the oxidant concentration is illustrated in Figure 6, which indicates a saturation behaviour, and a fit of the data to equation 4 yields the values of *a* and *b* in Table 4. Although the spectrum calculated for intermediate B shows an absorption band at c.a. 420 nm (Figure S87), it cannot be ruled out that this band corresponds to some amount of remaining starting complex. The spectral changes in the next step are smaller and the values derived for k_{2obs} are independent of the concentration of H_2O_2, except for the case of complex **2**. The values of *a* and *b* in Table 4 indicate that there are no large differences in the kinetic parameters for the different systems studied, including the reference EUK-134 compound.

Comentado [M9]: aqui

$$k_{obs} = \frac{ab[\mathrm{Ox}]}{1 + b[\mathrm{Ox}]} \qquad (4)$$

Similar kinetic studies were carried out in water solution, in this case using both H_2O_2 and TBHP as oxidant. To make the results more comparable, the pH and temperature were

similar to those used in the tests of biological activity (37ºC, pH= 7.25). Although the lower solubility of the complexes in water forces the use of lower concentration of the complexes, significant spectral changes could be measured and they showed in all cases the disappearance of the bands of the starting complex with the appearance of new bands at 350 nm and 260 nm, thus indicating the occurrence of the same type of reaction for all the complexes. Typical changes and calculated spectra for the reaction of complex **2** with H_2O_2 are included in Figures S9- S10, and for the reaction of **2** with TBHP in Figures S11-S12. In all cases, the spectral changes can be satisfactorily fitted with a single kinetic step, although at long reaction times there are additional small and irreproducible changes that lead to partial disappearance of the bands formed in the previous step. It is important to note that the complexes do not react with the buffer solution in the time in which the reaction with the oxidants takes place. As observed in methanol, the values derived for the rate constant change with the concentration of oxidant with saturation behaviour (Figures 7 and S13), and the fit of k_{obs} to equation 4 leads to the values of *a* and *b* in Table 5. Again there are no large differences in the kinetics of reaction of the different Mn complexes.

Table 5. Summary of kinetic data for the reaction of the Mn complexes with H_2O_2 and TBHP in water solutions at 37ºC and pH= 7.25. For the meaning of *a* and *b* see equation 4.

	H_2O_2		**TBHP**	
Complex	***a*/s^{-1}**	***b*/M^{-1}**	***a*/s^{-1}**	***b*/M^{-1}**

1	$(1.1\pm0.1)\times10^{-3}$	$(6\pm1)\times10^{3}$	$(2.0\pm0.1)\times10^{-4}$	$(9\pm2)\times10^{3}$
2	$(2.1\pm0.2)\times10^{-3}$	$(4\pm1)\times10^{3}$	$(3.0\pm0.1)\times10^{-4}$	$(5.2\pm0.5)\times10^{3}$
3	$(2.6\pm0.1)\times10^{-3}$	$(1.0\pm0.2)\times10^{3}$	$(2.0\pm0.1)\times10^{-4}$	$(1.3\pm0.3)\times10^{3}$
EUK-134	$(1.7\pm0.2)\times10^{-3}$	$(5\pm1)\times10^{3}$	$(3.0\pm0.1)\times10^{-4}$	$(6\pm1)\times10^{3}$

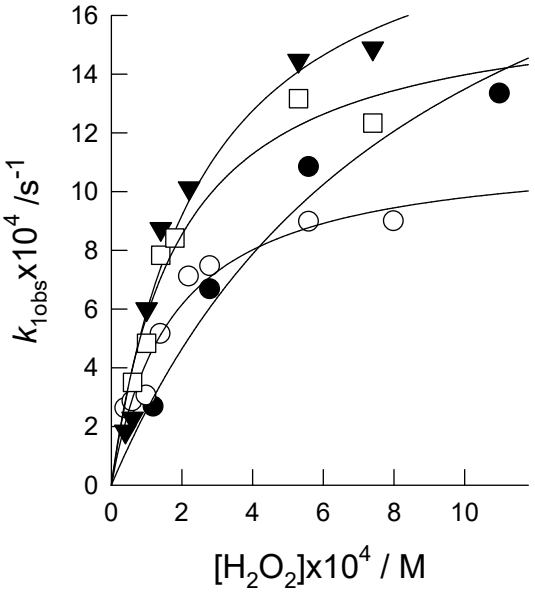

Figure 7. Plot of the [H_2O_2] dependence of the observed rate constant in the reaction of the Mn complexes with H_2O_2 in water solution at 37ºC and pH= 7.25: **1** (empty circles), **2** (triangles), **3** (filled circles) and **EUK-134** (squares).

The operation of free radical processes in acetonitrile solution has been reported previously [23], but some comment must be made at this point about the reaction mechanism and the nature of the intermediates and products formed in methanol and water solution in the reaction with H_2O_2 and TBHP. Previous reports suggest that the reaction of this kind of Mn^{III} complexes with H_2O_2 leads initially to the formation of $Mn^{V}(O)$ intermediates [10,45] but those oxo species can evolve to other species depending on the reaction conditions, and the band observed at 350 nm could correspond to a new Mn(III) complex formed from an initial Mn(V)=O product [46].In any case, although further work is required to ascertain the nature of the species formed, the present kinetic results clearly indicate the reaction of the Mn complexes with H_2O_2, and the experiments on their CAT activity indicate the operation of a catalytic cycle for H_2O_2 disproportionation, which probably occurs through the previously proposed mechanism [10]. In that mechanism, H_2O_2 attacks to the Mn(III) complex with formation of a Mn(V) intermediate that reacts with a second molecule of H_2O_2 to regenerate the starting complex with O_2 release. Moreover, the observation that most of the gases evolve in the CAT studies in the first 5-10 minutes agrees well with the half times calculated from the limiting rate constant (*a* in equation 4) in the kinetic studies in methanol and water (3-10 minutes for the different complexes), thus suggesting that the values of *a* can be associated to the rate-determining step in the CAT cycle. The absence of a detectable $Mn^{V}(O)$ intermediate also suggests that the rate determining step is the initial reaction with H_2O_2; although the resulting $Mn^{V}(O)$ intermediate would not accumulate because it is very reactive towards H_2O_2 and so it would be formed under steady-state conditions. However, as the catalytic cycle regenerates the Mn(III) complex, an additional process must be included in the mechanism to account for the disappearance of the starting complex. The

resulting mechanism is included in Scheme 2, and application of the steady-state approximation to the Mn(V) intermediate leads to the rate law in eq 5, which is of the same form that eq 4 with the equivalencies in eqs 6-7.

$$k_{obs} = \frac{k_{1a}k_{2b}[H_2O_2]}{k_{2b}+k_{2a}[H_2O_2]} \qquad (5)$$

$$a = \frac{k_{1a}k_{2b}}{k_{2a}} \qquad (6)$$

$$b = \frac{k_{2a}}{k_{2b}} \qquad (7)$$

Finally, one might wonder why the reaction with H_2O_2 in acetonitrile behaves so different from that in methanol and water. In acetonitrile the reaction is dominated by free radical processes initiated by photochemical processes, and the reaction under conditions similar to those used in methanol and water show an induction period that indicates that the k_{1a} step in Scheme 1 (k_{1a} step) is inhibited and the reaction only starts when free radicals are generated. With the information currently available it is not possible to give a definitive explanation but one possibility is that acetonitrile coordination stabilizes the Mn^{III} state hindering oxygen transfer from H_2O_2 but allowing free radical oxidation to Mn^{IV}. Another possibility is that the process defined by k_{1a} require in some way participation of a protic solvent to favor hydrogen bonding or proton transfer. It is evident that further work is required to shed light on the intimate mechanistic features of these reactions.

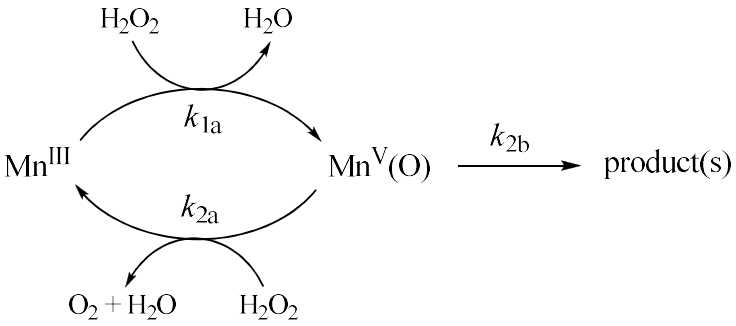

Scheme 2

4. CONCLUSIONS

A carefully selection and design of the ligands is a key issue to get active antioxidant biomimetic models. For the case of the *salen*-type ligands, the $2N_{imine}2O_{phenoxy}$ core forms an inner cavity that can accommodate the manganese ion. Extra methoxy atoms, which point toward the outside of the inner cavity, facilitates an extension of the dimensionality of the structure. The tetragonal elongation of the octahedral structure may be forced by the selection of the appropriate ligands.

In this work, we demonstrated for the first time the neuroprotective effects of this type of biomimetic models against oxidative stress in a human neuronal model. Complexes **1**-**3** significantly improved the cell viability loss induced by TBHP. The reaction mechanism for **1**-**3** versus a common oxidant as hydrogen peroxide is strongly dependent on the conditions. Solvent media, illumination conditions and other factors may vary not only the antioxidant activity but also the reaction mechanism itself.

Kinetic data in buffered solutions are in line with the results of the oxidative stress studies on SH-SY5Y cells and also with the results of the CAT activity test. All the complexes studied, including the commercial EUK-134, show a rate determining step in the catalytic cycle that corresponds to the initial reaction of the complexes with H_2O_2. Rate constants obtained for complexes **1**-**3** and EUK-134 being comparable, which could allow the use of the new complexes in antioxidant applications similar to the commercial compound.

Acknowledgements

The research leading to these results has received funding from the following FEDER cofunded-grants. From Consellería de Cultura, Educación e Ordenación Universitaria, Xunta de Galicia, 2017 GRC GI-1682 (ED431C 2017/01), 2018 GRC GI-1584 (ED431C 2018/13), MetalBIO Network (ED431D 2017/01). From CDTI and Technological Funds, supported by Ministerio de Economía, Industria y Competitividad, CTQ2015-65707-C2-2-P, AGL2016-78728-R (AEI/FEDER, UE), ISCIII/PI16/01830 and RTC-2016-5507-2, ITC-20161072. From European Union POCTEP 0161-Nanoeaters -1-E-1, Interreg AlertoxNet EAPA-317-2016, Interreg Agritox EAPA-998-2018, and H2020 778069-EMERTOX.

Appendix A- Supplementary data

Supplementary data associated with this article can be found, in the online version, at http://dx.doi.org/10.1016/j.jinorgbio.xxx.

References

[1] F. A. Villamena, Chemistry of Reactive Species, in: F. A. Villamena (Ed.), Molecular Basis of Oxidative Stress, Ed. John Wiley & Sons, New Jersey, 2013, pp.1-48.

[2] M. Oszajca, M. Brindell, L. Orzel, J.M. Dabrowski, K. Spiewak, P. Labuz, M. Pacia, A. Stochel-Gaudyn, W. Macyk, R. van Eldik, G. Stochel, Coord. Chem. Rev. 143 (2016) 327-328.

[3] M.T. Lin, M.F. Beal, Nature 443 (2006) 787–795.

[4] P. Sharma, P. Srivastava, A. Seth, P.N. Tripathi, A.G. Banerjee, S.K. Shrivastava, Progress in Neurobilogy 174 (2019) 53-89.

[5] B. DeStrooper, E. Karran, Cell 164 (2016) 603–615.

[6] C. Patterson, World Alzheimer Report 2018, New Frontiers, London, 2018, 32-36.

[7] S. Signorella, C. Palopoli, G. Ledesma, Coord. Chem. Rev. 365 (2018) 75-102.

[8] B. A. Baglia, J.P.T. Zaragoza, D.P. Goldberg, Chem. Rev. 117 (2017) 13320-13352.

[9] H.Y.V. Ching, I. Kenkel, N. Delsuc, E. Mathieu, I. Ivanovic-Burrnazovic, C. Policar, J. Inorg. Biochem. 160 (2016) 172-179.

[10] S.R. Doctrow, K. Huffman, C.B. Marcus, G. Tocco, E. Malfroy, C.A. Adinolfi, H, Kruk, K. Baker, N. Lazarowych, J. Mascarenhas, B. Malfroy, *J. Med. Chem*. 45 (2002) 4549-4558.

[11] M. Baudry, S. Etienne, A. Bruce, M. Palucki, E. Jacobsen, B. Malfroy, *Biochem. Biophys. Res. Commun.* 192 (1993) 964-968.

[12] J.C. Kash, Y. Xiao, A. Sally Davis, K.A. Walters, D.S. Chertow, J.D. Easterbrook, R.L. Dunfee, A. Sandouk, B.W. Jagger, L.M. Shwartzman, R.E. Kuestner, N.B. Wehr, K.

Huffman, R.A. Rosenthal, A. Ozinsky, R.L. Levine, S.R. Doctrow, J.K. Taubenberger, *Free Radic. Biol. Med. 67 (*2014) 235-247.

[13] S.R. Doctrow, K. Huffman, C.B. Marcus, W. Musleh, A. Bruce, M. Baudry, B. Malfroy, *Adv. Pharmacol*. 38 (1997) 247-269.

[14] C. Palopoli, G. Gómez, A. Foi, F. Doctorovich, S. Mallet-Ladeira, C. Hureau, S. Signorella, J. Inorg. Biochem. 167 (2017) 49-59.

[15] G.N. Ledesma, E. Anxolabéhère-Mallart, L. Sabater, C. Hureau, S.R. Signorella, J. Inorg. Biochem. 186 (2018) 10-16.

[16] M. Keener, M. Peterson, R.H. Sanchez, V.F. Oswald, G. Wu, G. Menard, *Chem. Eur. J. 23 (*2017) 11479-11484.

[17] D. Bani, A. Bencini, *Curr. Med. Chem.* 19 (2012) 4431-4444.

[18] S. Bahramikia, R. Yazdanparast, *Med. Chem. Res*. 21 (2012) 3224-3232.

[19] S.R. Doctrow, M. Liesa, S. Melov, O.S. Shirihai, P. Tofilon, *Current Inorg. Chem.* 2 (2012) 325-334.

[20] M.R. Bermejo, M.I. Fernández, E. Gómez-Fórneas, A. González-Noya, M. Maneiro, R. Pedrido, M.J. Rodríguez, J.C. García-Monteagudo, B. Donnadieu, J. Inorg. Biochem. 100 (2006) 1470-1478.

[21] M.A. Vázquez-Fernández, M.R. Bermejo, M.I. Fernández-García, G. González-Riopedre, M.J. Rodríguez-Doutón, M. Maneiro, J. Inorg. Biochem. 105 (2011) 1538-1547.

[22] G. González-Riopedre, M.R. Bermejo, M.I. Fernández-García, A.M. González-Noya, R. Pedrido, M.J. Rodríguez-Doutón, M. Maneiro, Inorg. Chem. 54 (2015) 2512-2521.

[23] A. Liberato, M.J. Fernández-Trujillo, Á. Máñez, M. Maneiro, L. Rodríguez-Silva, M.G. Basallote, Inorg. Chem. 57 (2018) 14471−14475.

[24] M.A. Vázquez-Fernández, M.I. Fernández-García, A.M. González-Noya, M. Maneiro, M.R. Bermejo, M.J. Rodríguez-Doutón, Polyhedron 31 (2012) 379-385.

[25] C. Palopoli, J. Ferreyra, A. Conte-Daban, M. Richezzi, A. Foi, F. Doctorovich, E. Anxolabéhère-Mallart, C. Hureau, S.R. Signorella, ACS Omega 4 (2019) 48-57.

[26] S.L. Huang, H.B. He, K. Zou, C.H. Bai, Y.H. Xue, J.Z. Wang, J.F. Chen, J Pharm Pharmacol 66 (2014) 844–854.

[27] R. Alvariño, E. Alonso, M.A. Tribalat, S. Gegunde, O.P. Thomas, L.M. Botana, Neurotox. Res. 32 (2017) 368-380.

[28] U. Casellato, P. Guerriero, S. Tamburini, P.A. Vigato, C. Benelli, *Inorg. Chim. Acta*. 207 (1993) 39-58.

[29] G. González-Riopedre, M.I. Fernández-García, E. Gómez-Fórneas, M. Maneiro, *Catalysts* 3 (2013) 232-246.

[30] M. R. Bermejo, R. Carballido, M. I. Fernández-García, A. M. González-Noya, G. González-Riopedre, M. Maneiro, L. Rodríguez-Silva, J. Chem. (2017) ID 5465890.

[31] J.M. McCord, I. Fridovich, J. Biol. Chem. 244 (1969) 6049-6055.

[32] E. Vega-Avila, M.K. Pugsley, Proc West Pharmacol Soc 54 (2011) 10–14.

[33] R.A. Binstead, B. Jung, A.D. Zuberbu̇hler, SPECFIT-32;Spectrum Software Associates, Chappel Hill, 2000.

[34] G.M. Sheldrick in “SHELX-97 (shelxs 97 and shelxl 97), Programs for Crystal Structure Analyses”, University of Göttingen, Germany, 1998.

[35] G. M. Sheldrick in “SADABS, Program for Scaling and Correction of Area Detector Data”, University of Göttingen, Germany, 1996.

[36] W.J. Geary, Coord. Chem. Rev. 7 (1971) 81-122.

[37] M. Zampakou, V. Tangoulis, C. P. Raptopoulou, V. Psycharis, A. N. Papadopoulos, G. Psomas, Eur. J. Inorg. Chem. 13 (2015) 2285-2294.

[38] A. Majumder, G. Pilet, M. T. Garlan, S. Mitra, Polyhedron 25 (2006) 2550-2558.

[39] M. Collomb, C. Mantel, S. Romain, C. Duboc, J. Lepetre, J. Pecaut, Eur. J. Inorg. Chem. (2007) 3179-3187.

[40] M. Navarro, C. A. Smith, M. Li, S. Bernhard, M. Albrecht, Chem. Eur. J. 24 (2018) 6386-6398.

[41] E. C. Constable, C. E. Housecroft, P. Kopecky, E. Schonhofer, J. A. Zampese, CrystEngComm 13 (2011) 2742-2752.

[42] D. H. Williams, E. Stephens, D. P. O'Brien, M. Zhou, Angew. Chem. Int. Ed. 43 (2004) 6596-6616.

[43] H. Zhang, M. Gao, L. Zhang, Y. Zhao, L.-L. Shi, B. Chen, Y. Wang, S. Wang, G. Du, Biochem. Biophys. Res. Commun. 421 (2012) 479– 483.

[44] W. Zhao, H. Feng, W. Sun, K. Liu, J.-J. Liu, X. Chem, Redox Biol. 11 (2017) 524-534.

[45] V. Lanza, G. Vecchio, J. Inorg. Biochem. 103 (2009) 381–388.

[46] K. Srinivasan, P. Michaud, J. K. Kochi, J. Am. Chem. Soc. 108 (1986) 2309-2320.